NANO LETTERS

pubs.acs.org/NanoLett Letter

Stiffer Is Stickier: Adhesion in Elastic Nanofilms

Chuanli Yu, Weijia Zeng, Bingjie Wang, Xuwei Cui, Zhida Gao, Jun Yin, Luqi Liu, Xianlong Wei, Yueguang Wei, and Zhaohe Dai*

Cite This: *Nano Lett.* 2025, 25, 1876−1882 Read Online

ACCESS | Metrics & More | Article Recommendations | Supporting Information

ABSTRACT: When two objects are brought into contact, separating them typically requires overcoming a detachment force. While this adhesion-induced force is vital for thin film materials in a range of nature and engineering systems, its quantitative understanding remains elusive due to the complex interplay between nonlinear deformation and adhesion. Here we perform controlled experiments and develop formal theories for the detachment force in a canonical configuration: separation of a sphere from an elastic graphene film. We observe that applying tension to the film can increase both its apparent out-of-plane stiffness and its detachment force, a behavior that cannot be explained by macroscopic adhesion theories. We attribute this unusual "stiffer-stickier" behavior to long-range intermolecular forces and demonstrate that it is a general phenomenon for elastic nanofilms, explainable through a multiscale theory that we develop. The ideas introduced here offer a generic strategy to understand the adhesion of slender structures across various length scales.

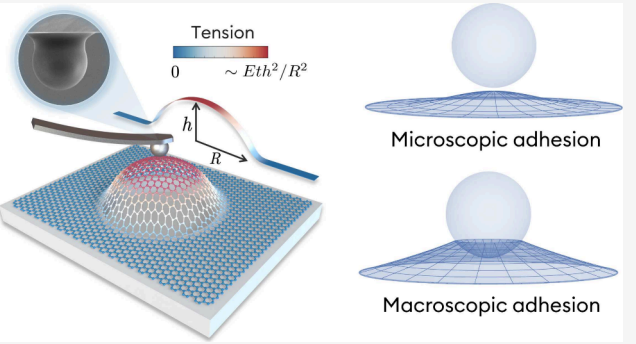

KEYWORDS: *Thin films, Detachment force, Adhesion, Graphene, Delamination*

Everyday experience teaches us that a critical force is required to detach an object from a sticky surface. This detachment force, resulting from adhesion, is particularly important for thin film materials due to their mechanical compliance and large surface-to-volume ratios.[1] Indeed, whether it is adhering a bandage onto skin,[2,3] closing wounds with a tape in surgeries,[4,5] preventing stiction in MEMS,[1,6] or the cellular uptake of nanoparticles,[7] the functionality of thin films relies on the proper utilization or overcoming of detachment forces. Recently, in fields such as condensed matter physics and mechanobiology, there have been increasingly sophisticated measurements of detachment forces in thin films.[8,9] Examples include detaching microprobes from 2D materials to understand the nature of van der Waals interactions[10−12] and detaching a nanocarrier from a cell membrane to appreciate its affinity.[9,13−16]

Despite its ubiquity, the detachment force in thin films remains poorly understood. A simple thought experiment with sticky bandages illustrates this gap (Figure 1A). When the bandage is pressed, the tensioned film feels stiffer than in its relaxed state. However, as the finger is lifted, the effect of the tension on the detachment force becomes less apparent. While reduced deflection in the tensioned film is noticeable at detachment, it is difficult to determine whether tension makes detachment any easier. Precise tests using polydimethylsiloxane (PDMS) films and a steel sphere show that the film stiffens; yet, somewhat unexpectedly, the detachment force remains nearly unchanged even when the film is strained up to 40% (Figure 1B). Unlike elastic slabs, interpreting the detachment force in thin elastic films is more challenging due to the nonlinear deformations involved. Consequently, across various thin film systems—ranging from polymeric sheets and cell membranes to atomically thin 2D materials[1,8−10]—the detachment force is often measured with precision but remains poorly interpreted.

To address this gap and provide a comprehensive understanding of what the detachment force can indicate for thin films, we propose controlled experiments on a canonical configuration—detaching a sphere from an ultrathin elastic film. We use 2−4 layered graphene sheets as model elastic films to investigate the detachment forces previously observed in small-scale films. Tension is extremely important in ultrathin materials, and to control it—since directly stretching 2D materials without support is highly challenging—we apply transverse pressure to induce shallow graphene bubbles, each characterized by radius R and height h (Figure 2A, see Supporting Information, Figure S2). The membrane tension T introduced this way is equal-biaxial at the center of the bubble

Received: October 24, 2024
Revised: December 26, 2024
Accepted: December 27, 2024
Published: December 31, 2024

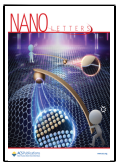

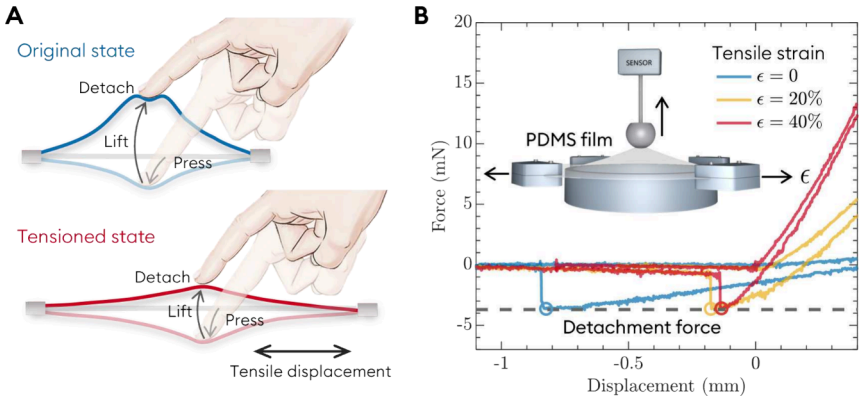

Figure 1. Detachment force in macroscopic elastic films. (A) Schematic demonstration of the detachment force examined by detaching the finger from a bandage. One may readily gauge that the applied tension can stiffen the elastic film but is unlikely to sense how it would change the detachment force. (B) Force−displacement curves measured by indenting a sphere on a thin PDMS film and then retracting the sphere back. The applied tension leads to a reduced detachment displacement but does not discernibly change the detachment force (pointed by the dashed line).

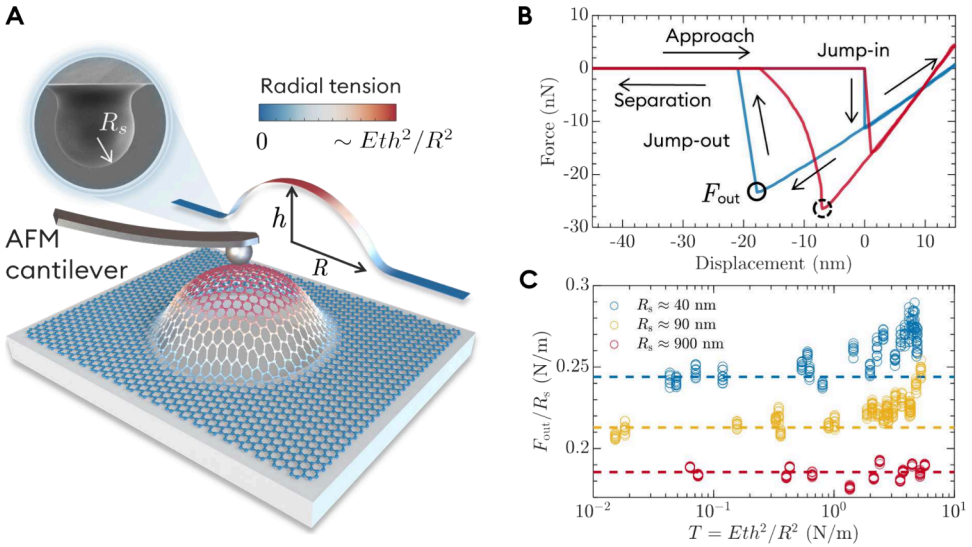

Figure 2. Detachment forces in tensioned nanofilms. (A) Schematic of the experimental setup in which a microsphere is brought into contact with a pressurized nanofilm. The applied tension, scaling as Eth^2/R^2, is nearly equal-biaxial around the center of the bubble. (B) Typical loading force−displacement curves measured during the approach and retraction process using a sphere with radius around 90 nm. The blue and red curves are measured from untensioned and tensioned nanofilms, respectively. (C) The measured detachment force (divided by the radius of the sphere) as a function of the applied tension to the film. The dependency on the sphere radius should be attributed to the fact that spheres of different radii are fabricated from different materials and techniques.

and scales as Eth^2/R^2 (ranging from ∼0.02 to 8.5 N/m in our experiments, since the bubble heights range from 5 to 240 nm for $R \approx 2800$ nm, and from 5 to 140 nm for $R \approx 1800$ nm), where E and t represent the Young's modulus and thickness of the film, respectively.[17,18] We show that unlike the macroscopic experiments in Figure 1B, applying tension to nanofilms can increase both their apparent stiffness and detachment force.

Measurement of detachment forces. Atomic force microscopy (AFM) is used to measure the detachment force in tensioned graphene films. We customize the AFM probe with microspherical tips of three distinct radii R_s: approximately 40, 90, and 900 nm (Supporting Information, Figure S3). To achieve this, we use three different fabrication methods, and the tip materials are silicon nitride, diamond-like carbon, and silicon dioxide, respectively (see Methods). Note that the curvature of all spheres, $1/R_s$, is much greater than that of the pressurized bubble ($\sim h/R^2 < \sim 10^{-4}$ nm^{-1}), making the influence of the bubble curvature induced by pressure (whether positive or even negative, see Supporting Information, S1.F) negligible in the experimental results presented later. However, it is important to emphasize that under significantly high pressures the pressure force and the bubble curvature could become critical to the detachment force.

In Figure 2B, we present typical force−displacement curves measured during the approach and retraction of the microsphere. As the sphere moves toward the film, a distinct snap-through phenomenon is observed, characterized by a sudden shift in the loading force to a negative value. This marks the jump-into-contact.[19] The further approach increases the loading force into the positive range, in which the poking stiffness of the film can be indicated. Retraction begins once the force threshold (1−5 nN) is reached. During retraction, the force−displacement curve does not fully follow the same path as that during approach. Particularly, it passes through the earlier snap-through point and reaches another minimum, after

https://doi.org/10.1021/acs.nanolett.4c05309
Nano Lett. 2025, 25, 1876−1882

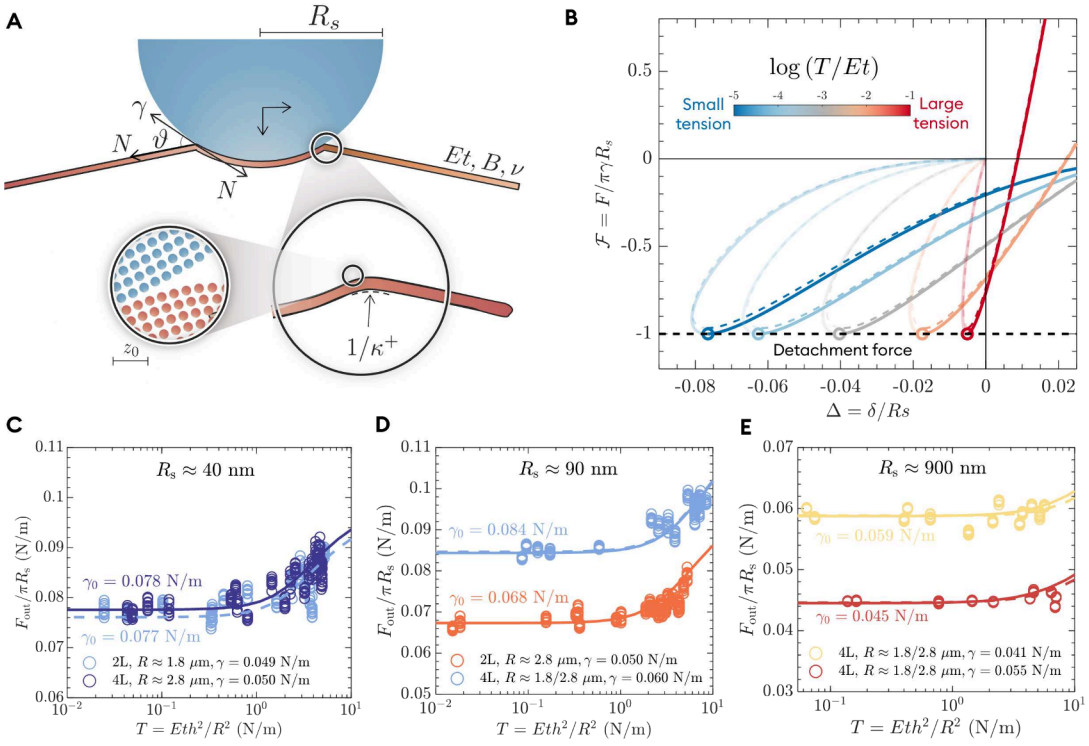

Figure 3. Multiscale adhesion of elastic nanofilms. (A) Schematic of the adhesion conditions across different scales. (B) The force−displacement relations calculated for various applied tension T. The solid curves are based on membrane theory, while the dashed curves are calculated with nonlinear plate theory (using $B/EtR^2 = 10^{-8}$). Line color is used to encode dimensionless tension, as in the associated color bar. The circle makers highlight the theoretically calculated detachment force. Note that the partially transparent part of each curve is not stable and hence cannot be observed in experiments. (C−E)The detachment force as a function of the applied tension for three different sphere radii. The solid (for $R = 2800$ nm) and dashed (for $R = 1800$ nm) curves are calculated with the microscopic model with the solid−solid adhesion γ being the fitting parameter. The nominal adhesion γ_0 is obtained by plugging the detachment force measured at small tension into the macroscopic model (eq 1).

which the sphere jumps out of contact with the film. This local minimum defines the detachment force F_{out}, which is insensitive to the specific loading force threshold (Supporting Information, Figure S4).

We then reveal how the mechanical and adhesive behaviors of the film depend on the tension applied to the film. As expected, when the film is tensioned, its apparent poking stiffness increases and the pulling displacement at the moment of detachment decreases (Figure 2B). However, somewhat counterintuitively, the detachment force increases, i.e., the nanofilm appears stickier when tensioned. More comprehensive results are provided in Figure 2C, showing that detachment forces measured with small spheres (approximately 40 or 90 nm in radius) increase monotonically with the applied tension. By contrast, experiments using a relatively large sphere ($R_s \approx 900$ nm) in Figure 2C and the macroscopic steel sphere in Figure 1B show detachment forces that are almost invariant with tension. This intriguing "stiffer-stickier" behavior and its size dependency have not been reported previously.

Macroscopic view of adhesion. To understand the unusual adhesion behavior observed, we first recall Shanahan's model for detaching a rigid sphere from a largely prestretched film.[20] In this model, the film behaves akin to a soap film with the detachment force given by[21−23]

$$F_{out} = \pi\gamma R_s \tag{1}$$

where γ is the solid−solid adhesion. By applying measured detachment forces in Figure 3C−E to (eq 1), we obtain γ values ranging from 50 to 100 mJ/m^2. Though this range is of the correct order of magnitude,[8] the Shanahan model suggests that the detachment force is independent of the tension or elastic stiffness of the film, which is inconsistent with our experimental finding. Clearly, the inherent elasticity of graphene films sets them apart entirely from the fluid nature of soap films, making the Shanahan model inapplicable.

We then turn our attention to elastic films for which, to our knowledge, a detachment force model has yet to be developed. We employ the classical Föppl membrane theory to describe the nonlinear elasticity of graphene films[24] and examine adhesion from a macroscopic perspective. In this context, creating a contact region of radius a, depicted in Figure 3A, results in a loss of adhesion energy ($\pi\gamma^2$) within the total free energy. Interfacial friction is disregarded due to the lubrication nature of graphene.[8] Through a variational analysis with a no-pinning condition (Supporting Information, S2), we find that adhesion can cause a kink in the thin film at the periphery of the contact region, or the "contact line" (Figure 3A):

$$s^- - s^+ = (2\gamma/N)^{1/2} \tag{2}$$

where $s^\pm$ is the slope of the film evaluated at the outer and inner side of the contact line, respectively, and N is the membrane tension developed at the contact line. We note that this critical condition can also be derived using Griffith's fracture mechanics by considering the energy release rate. Such a condition can also be interpreted in terms of an adhesive contact angle, given by $\cos\theta = (N - \gamma)/N$, as illustrated in the first-order view in Figure 3A.

https://doi.org/10.1021/acs.nanolett.4c05309
Nano Lett. 2025, 25, 1876−1882

With this contact angle, we are able to solve the force−displacement relations for various tensions $T = Eth^2/R^2$, which are adjusted by the applied pressures from the first principle (Supporting Information, S2). The calculated results are presented as colored solid curves in Figure 3B. As expected, increasing the applied tension "facilitates" the detachment of the sphere from the film by reducing the required detachment displacement (marked by circles in Figure 3B). However, the required detachment force remains unaffected by the applied tension. This implies that the increase in the membrane tension is somehow balanced by the decrease in the adhesive contact angle. Consequently, it just so happens that $F_{out} = \pi\gamma R_s$, as predicted by the Shanahan model, works for elastic films under any applied tension, leaving the mechanism of the tension-dependent detachment forces unclear.

We further include the bending effect of the film that has hitherto been neglected (Supporting Information, S2). This consideration prevents the film from forming a kink or contact angle. However, observing the system on the scale of $(B/N)^{1/2}$,[25] adhesion can still result in a discontinuity that instead arises in the curvature of the film (see the second-order view in Figure 3A), given by

$$\kappa^- - \kappa^+ = (2\gamma/B)^{1/2} \tag{3}$$

where $\kappa^{\pm}$ is the curvature of the film outside and inside the contact line, and B is the bending stiffness of the film.[26] We find that using a finite B can lead to a reduction in F_{out}, but the detachment force remains almost invariant with respect to the applied tension (dotted curves in Figure 3B). In addition, for highly bendable nanofilms used in our experiments, this reduction is negligible (as summarized in Supporting Information, Figure S6), suggesting that the bending effect cannot explain the "stiffer-stickier" behavior either. The question now is what has prevented the macroscopic view of adhesion from explaining the tension-dependent detachment forces in thin films.

Microscopic view of adhesion. Motivated by the Greenwood adhesion theory for elastic slabs,[27] we zoom in further on the "contact line" to the molecular level. From this perspective, the contact-to-detachment transition looks smooth rather than abrupt, as illustrated in the third-order view in Figure 3A. Consequently, the sharp changes in the slope or curvature of the film required by macroscopic models do not occur. To better characterize the film-sphere interface, we instead utilize the long-range interfacial van der Waals forces p_{vdW}:[27]

$$p_{vdW}(s) = \frac{8\gamma}{3z_0}\left[\left(\frac{z_0}{s}\right)^3 - \left(\frac{z_0}{s}\right)^9\right] \tag{4}$$

where s is the gap between the sphere and the tensioned nanofilm, and z_0 represents the equilibrium spacing between two solid surfaces. In this microscopic model, the interfacial traction is zero at $s = z_0$, and separating the interface from equilibrium to infinity requires an energy of γ per unit area.

The detachment force is then computed by using these long-range interfacial forces. Figure 3C−E presents two typical data sets obtained with spheres of three distinct radii. In each data set, measurements are conducted using the same batch of exfoliated graphene films and the same sphere, ensuring that applied tension is the sole variable. We find excellent agreement between the results from calculations and experiments, enabling the extraction of the "true" solid−solid adhesion γ. Notably, one might combine the macroscopic model and the detachment forces measured under small tensions to estimate a "nominal" adhesion energy, $\gamma_0 = F_{out}/\pi R_s$. Such an γ_0, however, is significantly higher than the true adhesion γ unless the radius of the testing sphere is large (Figure 3C−E). This implies that the difference between macroscopic and microscopic models is actually reduced with the increase in sphere size. We then discuss the conditions under which adhesion in elastic nanofilms can be considered macroscopic or macroscopic, which would provide a physical picture of why detachment forces are larger in stiffer or smaller systems.

A transition parameter. On one hand, when the apparent stiffness of the film upon pulling or poking is sufficiently large, the film's deflection is limited so that z_0 at the interface provides the only vertical length scale of the system (Figure 4A). Such a scenario is expected for films with high intrinsic

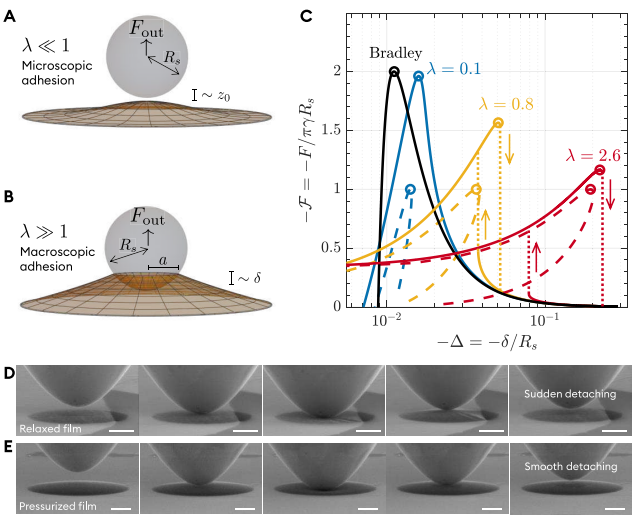

Figure 4. Microscopic adhesion of elastic nanofilms. Schematic illustration of the adhesion model for thin films with small (A) and large (B) deformability. The key difference lies in that large tension or elastic stiffness would prevent the establishment of a well-defined contact area between the sphere and the film. (C) The apparent paradox in the detachment force (marked by circles) between Bradley's rigid body limit (black curve) and the macroscopic model (dashed curves) can be resolved by the microscopic model with a transition parameter λ (colored solid curves). The vertical dotted lines in the case of $\lambda \sim 1$ denote the snap-through instability as the sphere approaches (toward $-x$ direction) and separates (toward $+x$ direction) from the film. (D,E) In situ SEM observation of the approaching and detaching process of a partially suspended (D) and pressurized (E) graphene film. The detaching action is sudden in (D), while it is relatively smooth in (E). Scale bars in (D,E): 1 μm.

stiffness or films with large applied tensions. On the other hand, for relatively compliant thin films under moderate tension (Figure 4B), it is reasonable to adopt the macroscopic view of adhesion. In this scenario, a contact region of radius a is established, in which the adhesion force deforms the elastic film by some deflection δ. The geometry dictates $\delta \sim a^2/R_s$. The loss of surface energy ($\sim\gamma a^2$) is compensated by the gain in elastic energy ($\sim T_{tot}\delta^2/a^2 \times a^2 = T_{tot}\delta^2$), where the total tension in the film T_{tot} is the sum of the applied tension T and the deflection-induced tension ($\sim Et\delta^2/a^2 \sim \sqrt{\gamma Et}$). These considerations lead to a characteristic vertical length, $\delta_* = \gamma R_s/T_{tot}$. We then define a transition parameter by comparing the lengths derived from these two distinct scenarios:

https://doi.org/10.1021/acs.nanolett.4c05309
Nano Lett. 2025, 25, 1876−1882

$$\lambda = \frac{\gamma R_s}{z_0(T + \sqrt{\gamma E t})} \quad (5)$$

This transition parameter helps us determine whether adhesion can be considered macroscopic ($\lambda \gg 1$) or microscopic ($\lambda \ll 1$). Evidently, when using small spheres or stiff films (achieved through either large applied tension T or intrinsic stiffness Et), the system features a small λ and is expected to exhibit microscopic adhesion behavior. In a limiting case of rigid films ($\lambda \to 0$), the summation of long-range interfacial forces between two surfaces leads to $F_{out} = 2\pi\gamma R_s$, known as Bradley's rigid body limit.[28] This result is twice as large as that of $F_{out} = \pi\gamma R_s$ in the macroscopic model. Therefore, the stiffer-stickier mechanism might be attributed to the fact that increasing the tension in the nanofilm makes it appear more rigid, causing its adhesion behavior to become more microscopic and enhancing the detachment force.

To further demonstrate this microscopic-to-macroscopic transition, we use the long-range interfacial force law to reproduce the pulling-force displacement curves in Figure 4C. Note that the upward pulling force/displacement is defined negatively relative to the pushing indentation. For demonstration purposes, we followed experiments using bilayer graphene sheets of R = 1.8 μm, R_s = 90 nm, z_0 = 1 nm, and γ = 1 N/m. The transition parameter λ is adjusted only by applied tension $T = Eth^2/R^2$. We find this microscopic model approaches Bradley's rigid body limit as $\lambda \ll 1$ (Figure 4C). With increasing λ, the pulling-force−displacement curve shows a decreased detachment force and gradually approaches the colored dashed curves, which are the macroscopic results reproduced from Figure 3B. While λ has an upper limit in Figure 4C (or in experiments) due to the fixed γ and nonvanishing film stiffness Et, we can achieve an arbitrary λ by tuning the value of γ in computation. It is found that F_{out} can consistently approach $2\pi\gamma R_s$ for small λ and $\pi\gamma R_s$ for large λ (Supporting Information, Figure S8). With such self-consistency, our macroscopic and microscopic adhesion models, together with the transition parameter, complete the adhesion theory for thin elastic films, which has been absent in the literature.

The results shown in Figure 4C also reproduce the jump-into and jump-out-of-contact instabilities, as indicated by the dotted lines. Interestingly, these instabilities occur only in relatively macroscopic systems, specifically when $\lambda \gtrsim 0.2$, which agree qualitatively with the observation in Figure 2B. Note that a quantitative understanding is challenging, as it needs detailed stability analysis incorporating with the AFM cantilever stiffness. The pulling displacement at the onset of the jump out of contact instability increases for systems of larger λ (i.e., more compliant films). This result is consistent with our intuition as well as in situ SEM experiments comparing a relaxed film and a tensioned film (Figure 4D,E). The relaxed (and thus complaint) film exhibits noticeable pulling displacement and sudden jump-out behavior at the detachment. In contrast, these features are barely observable in the tensioned (and consequently stiffer) film (see a qualitative comparison in Supporting Information Video 1).

In Figure 5, we summarize all measured data against their transition parameters, estimated by using γ = 50 mJ/m^2. The essence of the "stiffer-stickier" phenomenon can now be understood: applied tension can stiffen the film, thereby reducing its transition parameter and making its adhesion behavior more microscopic. This effect is particularly pronounced with small spheres (with $R_s \approx$ 40 and 90 nm). Alternatively, when $R_s \approx$ 900 nm, the transition parameter remains much greater than 1 even under applied tension. In these cases, the adhesion is more macroscopic and the detachment force appears tension-independent. An important implication for future experiments involving contact and detachment with nanofilms is that the simpler macroscopic model discussed here can be effectively used as long as a large transition parameter is ensured in experiments.

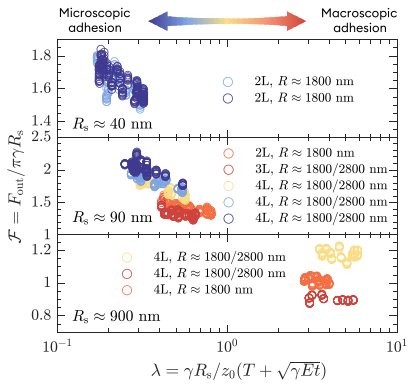

Figure 5. Interpreting the detachment force with a transition parameter. Measured detachment forces are a function of the transition parameter. The data with the same color in each panel were measured from the same batch of samples with the same microsphere. We note that combining these results into a master relation is challenging due to the differences in material systems and the inherent complexity of λ.

Although this study focuses on graphene films, the concepts introduced here provide a general framework for understanding the adhesion of other slender materials and structures. The phenomenon of finite detachment forces has been observed across a broad range of slender materials at various length scales,[29] including 2D materials,[30,31] polymeric films,[32,33] nanowires,[34,35] living cells,[36,37] and biotissues.[38,39] Previous interpretations of such forces have relied on the classical Johnson−Kendall−Roberts (JKR) model,[14,36−38] which applies to bulk, compliant materials but is inadequate for slender structures. Additionally, in the case of bulk solids, there exists a well-known contradiction between the JKR model and Bradley's rigid body limit.[29] This discrepancy has been resolved by introducing the Tabor parameter, which compares the elastic deformation caused by adhesion to z_0.[29] In contrast, the transition parameter λ we introduce here is specifically tailored for thin films. While geometric nonlinearity presents intriguing challenges, it is reassuring to observe conceptual parallels with the classical Tabor parameter, such as the λ-dependence of detachment forces, as shown in Figure 5.

■ ASSOCIATED CONTENT

Supporting Information

The Supporting Information is available free of charge at https://pubs.acs.org/doi/10.1021/acs.nanolett.4c05309.

Experimental methods, complementary experimental results, and theoretical modeling details that support the discussion in the main text (PDF)

Video of in situ detachment test on relaxed and tensioned graphene (MP4)

https://doi.org/10.1021/acs.nanolett.4c05309
Nano Lett. 2025, 25, 1876−1882

AUTHOR INFORMATION

Corresponding Author

Zhaohe Dai − *Department of Mechanics and Engineering Science, State Key Laboratory for Turbulence and Complex Systems, College of Engineering, Peking University, Beijing 100871, China;* orcid.org/0000-0002-5205-089X; Email: daizh@pku.edu.cn

Authors

Chuanli Yu − *Department of Mechanics and Engineering Science, State Key Laboratory for Turbulence and Complex Systems, College of Engineering, Peking University, Beijing 100871, China*

Weijia Zeng − *Department of Mechanics and Engineering Science, State Key Laboratory for Turbulence and Complex Systems, College of Engineering, Peking University, Beijing 100871, China*

Bingjie Wang − *Key Laboratory for the Physics and Chemistry of Nanodevices, School of Electronics, Peking University, Beijing 100871, China;* orcid.org/0000-0001-8397-3761

Xuwei Cui − *CAS Key Laboratory of Nanosystem and Hierarchical Fabrication, CAS Center for Excellence in Nanoscience, National Center for Nanoscience and Technology, Beijing 100190, China*

Zhida Gao − *State Key Laboratory of Mechanics and Control of Mechanical Structures, Nanjing University of Aeronautics and Astronautics, Nanjing, Jiangsu 210016, China*

Jun Yin − *State Key Laboratory of Mechanics and Control of Mechanical Structures, Nanjing University of Aeronautics and Astronautics, Nanjing, Jiangsu 210016, China;* orcid.org/0000-0003-3375-8160

Luqi Liu − *CAS Key Laboratory of Nanosystem and Hierarchical Fabrication, CAS Center for Excellence in Nanoscience, National Center for Nanoscience and Technology, Beijing 100190, China;* orcid.org/0000-0002-5752-1638

Xianlong Wei − *Key Laboratory for the Physics and Chemistry of Nanodevices, School of Electronics, Peking University, Beijing 100871, China;* orcid.org/0000-0002-1181-9500

Yueguang Wei − *Department of Mechanics and Engineering Science, State Key Laboratory for Turbulence and Complex Systems, College of Engineering, Peking University, Beijing 100871, China*

Complete contact information is available at: https://pubs.acs.org/10.1021/acs.nanolett.4c05309

Author Contributions

C.Y. and Z.D. designed the research; C.Y. conducted indentation experiments; W.Z. and Y.W. developed the theory and computations; B.W. and X.W. carried out SEM experiments; X.C. and L.L. contributed to the sample fabrication; Z.G. and J.Y. performed environmental AFM characterizations; C.Y., W.Z., and Z.D. wrote the paper. All authors discussed the results and commented on the manuscript.

Notes

The authors declare no competing financial interest.

ACKNOWLEDGMENTS

This work was financially supported by the National Natural Science Foundation of China (Grant No. 12372103, 12432003). We are grateful to Prof. Xiaoding Wei and Qunyang Li for their insightful and constructive suggestions.

REFERENCES

(1) Bico, J.; Reyssat, É.; Roman, B. Elastocapillarity: when surface tension deforms elastic solids. *Annu. Rev. Fluid Mech.* **2018**, *50*, 629−659.

(2) Box, F.; Domino, L.; Corvo, T. O.; Adda-Bedia, M.; Démery, V.; Vella, D.; Davidovitch, B. Delamination from an adhesive sphere: Curvature-induced dewetting versus buckling. *Proc. Natl. Acad. Sci. U. S. A.* **2023**, *120*, No. e2212290120.

(3) Liu, S.; He, J.; Rao, Y.; Dai, Z.; Ye, H.; Tanir, J. C.; Li, Y.; Lu, N. Conformability of flexible sheets on spherical surfaces. *Sci. Adv.* **2023**, *9*, No. eadf2709.

(4) Paulsen, J. D. Wrapping liquids, solids, and gases in thin sheets. *Annu. Rev. Condens. Matter Phys.* **2019**, *10*, 431−450.

(5) Yuk, H.; Varela, C. E.; Nabzdyk, C. S.; Mao, X.; Padera, R. F.; Roche, E. T.; Zhao, X. Dry double-sided tape for adhesion of wet tissues and devices. *Nature* **2019**, *575*, 169−174.

(6) Tas, N.; Sonnenberg, T.; Jansen, H.; Legtenberg, R.; Elwenspoek, M. Stiction in surface micromachining. *J. Micromech. Microeng.* **1996**, *6*, 385.

(7) Yi, X.; Shi, X.; Gao, H. Cellular uptake of elastic nanoparticles. *Phys. Rev. Lett.* **2011**, *107*, No. 098101.

(8) Dai, Z.; Lu, N.; Liechti, K. M.; Huang, R. Mechanics at the interfaces of 2d materials: Challenges and opportunities. *Curr. Opin. Solid State Mater. Sci.* **2020**, *24*, No. 100837.

(9) Krieg, M.; Fläschner, G.; Alsteens, D.; Gaub, B. M.; Roos, W. H.; Wuite, G. J.; Gaub, H. E.; Gerber, C.; Dufrêne, Y. F.; Müller, D. J. Atomic force microscopy-based mechanobiology. *Nat. Rev. Phys.* **2019**, *1*, 41−57.

(10) Li, B.; Yin, J.; Liu, X.; Wu, H.; Li, J.; Li, X.; Guo, W. Probing van der waals interactions at two-dimensional heterointerfaces. *Nat. Nanotechnol.* **2019**, *14*, 567−572.

(11) Rokni, H.; Lu, W. Direct measurements of interfacial adhesion in 2d materials and van der waals heterostructures in ambient air. *Nat. Commun.* **2020**, *11*, 5607.

(12) Li, S.; Li, Q.; Carpick, R. W.; Gumbsch, P.; Liu, X. Z.; Ding, X.; Sun, J.; Li, J. The evolving quality of frictional contact with graphene. *Nature* **2016**, *539*, 541−545.

(13) Friedrichs, J.; Helenius, J.; Muller, D. J. Quantifying cellular adhesion to extracellular matrix components by single-cell force spectroscopy. *Nat. Protoc.* **2010**, *5*, 1353−1361.

(14) Haase, K.; Pelling, A. E. Investigating cell mechanics with atomic force microscopy. *J. R. Soc. Interface* **2015**, *12*, 20140970.

(15) Chu, Y.-S.; Dufour, S.; Thiery, J. P.; Perez, E.; Pincet, F. Johnson-kendall-roberts theory applied to living cells. *Phys. Rev. Lett.* **2005**, *94*, No. 028102.

(16) Hu, J.; Youssefian, S.; Obayemi, J.; Malatesta, K.; Rahbar, N.; Soboyejo, W. Investigation of adhesive interactions in the specific targeting of triptorelin-conjugated peg-coated magnetite nanoparticles to breast cancer cells. *Acta Biomater.* **2018**, *71*, 363−378.

(17) Dai, Z.; Hou, Y.; Sanchez, D. A.; Wang, G.; Brennan, C. J.; Zhang, Z.; Liu, L.; Lu, N. Interface-governed deformation of nanobubbles and nanotents formed by two-dimensional materials. *Phys. Rev. Lett.* **2018**, *121*, 266101.

(18) Koenig, S. P.; Boddeti, N. G.; Dunn, M. L.; Bunch, J. S. Ultrastrong adhesion of graphene membranes. *Nat. Nanotechnol.* **2011**, *6*, 543−546.

(19) Yu, C.; Dai, Z. Premature jump-to-contact with elastic surfaces. *J. Mech. Phys. Solids* **2024**, *193*, 105919.

(20) Shanahan, M. E. Adhesion of a punch to a thin membrane. *C. R. Acad. Sci. Paris, Sér. IV, Phys.* **2000**, *1*, 517−522.

(21) Borodich, F. M.; Galanov, B. A. Contact probing of stretched membranes and adhesive interactions: graphene and other two-dimensional materials. *Proc. R. Soc. A: Math. Phys. Eng. Sci.* **2016**, *472*, 20160550.

(22) Yuan, W.; Wang, G. Adhesion between a rigid sphere and a stretched membrane using the dugdale model. *Int. J. Solids Struct.* **2021**, *208*, 214−220.

(23) Argatov, I. I. Indentation mapping of stretched adhesive membranes. *Proc. Royal Soc. A* **2021**, *477*, 20210349.

(24) Mansfield, E. H. *The bending and stretching of plates*, 2nd ed.; Cambridge University Press, 1989.
(25) Davidovitch, B.; Vella, D. Partial wetting of thin solid sheets under tension. *Soft Matter* **2018**, *14*, 4913−4934.
(26) Majidi, C.; Adams, G. G. A simplified formulation of adhesion problems with elastic plates. *Proc. R. Soc. A: Math. Phys. Eng. Sci.* **2009**, *465*, 2217−2230.
(27) Greenwood, J. Adhesion of elastic spheres. *Proc. R. Soc. A: Math. Phys. Eng. Sci. Series A: Mathematical, Physical and Engineering Sciences* **1997**, *453*, 1277−1297.
(28) Bradley, R. S. Lxxix. the cohesive force between solid surfaces and the surface energy of solids. *The London, Edinburgh, Dublin Philos. Mag. J. Sci.* **1932**, *13*, 853−862.
(29) Ciavarella, M.; Joe, J.; Papangelo, A.; Barber, J. The role of adhesion in contact mechanics. *J. R. Soc., Interface* **2019**, *16*, 20180738.
(30) López-Polín, G.; Gómez-Navarro, C.; Parente, V.; Guinea, F.; Katsnelson, M. I.; Perez-Murano, F.; Gómez-Herrero, J. Increasing the elastic modulus of graphene by controlled defect creation. *Nat. Phys.* **2015**, *11*, 26−31.
(31) Li, Y.; Huang, S.; Wei, C.; Wu, C.; Mochalin, V. N. Adhesion of two-dimensional titanium carbides (mxenes) and graphene to silicon. *Nat. Commun.* **2019**, *10*, 3014.
(32) Wang, G.; Najafi, F.; Ho, K.; Hamidinejad, M.; Cui, T.; Walker, G. C.; Singh, C. V.; Filleter, T. Mechanical size effect of freestanding nanoconfined polymer films. *Macromolecules* **2022**, *55*, 1248−1259.
(33) Wang, D.; Russell, T. P. Advances in atomic force microscopy for probing polymer structure and properties. *Macromolecules* **2018**, *51*, 3−24.
(34) Yang, L.; Tao, Y.; Zhu, Y.; Akter, M.; Wang, K.; Pan, Z.; Zhao, Y.; Zhang, Q.; Xu, Y.-Q.; Chen, R.; et al. Observation of superdiffusive phonon transport in aligned atomic chains. *Nat. Nanotechnol.* **2021**, *16*, 764−768.
(35) Ma, X.; Zhu, Y.; Kim, S.; Liu, Q.; Byrley, P.; Wei, Y.; Zhang, J.; Jiang, K.; Fan, S.; Yan, R.; et al. Sharp-tip silver nanowires mounted on cantilevers for high-aspect-ratio high-resolution imaging. *Nano Lett.* **2016**, *16*, 6896−6902.
(36) Obataya, I.; Nakamura, C.; Han; Nakamura, N.; Miyake, J. Nanoscale operation of a living cell using an atomic force microscope with a nanoneedle. *Nano Lett.* **2005**, *5*, 27−30.
(37) Mandriota, N.; Friedsam, C.; Jones-Molina, J. A.; Tatem, K. V.; Ingber, D. E.; Sahin, O. Cellular nanoscale stiffness patterns governed by intracellular forces. *Nat. Mater.* **2019**, *18*, 1071−1077.
(38) Zhu, D.; Liu, Y.; Gilbert, J. L. Micromechanical measurement of adhesion of dehydrating silicone hydrogel contact lenses to corneal tissue. *Acta Biomater.* **2021**, *127*, 242−251.
(39) Bouchonville, N.; Meyer, M.; Gaude, C.; Gay, E.; Ratel, D.; Nicolas, A. Afm mapping of the elastic properties of brain tissue reveals kpa μm- 1 gradients of rigidity. *Soft Matter* **2016**, *12*, 6232−6239.

https://doi.org/10.1021/acs.nanolett.4c05309
Nano Lett. 2025, 25, 1876−1882